Optical characterization of polar HfO_2 nanoparticles in the mid- and far-infrared

O. Dominguez,[1,a)] T. L. McGinnity,[2] R. K. Roeder,[2] and A. J. Hoffman[1]
[1]*Department of Electrical Engineering, University of Notre Dame, Notre Dame, Indiana 46556, USA*
[2]*Department of Aerospace and Mechanical Engineering, University of Notre Dame, Notre Dame, Indiana 46556, USA*

(Received 28 February 2017; accepted 20 June 2017; published online 5 July 2017)

Monoclinic HfO_2 nanoparticles with nominal diameters of 9, 30, and 45 nm are characterized using transmission and reflection spectroscopy from the mid- to far-infrared. Phonon modes are identified in the measured spectra and agree with previously reported values in HfO_2 thin films and density functional perturbation theory calculations. An anomaly in both reflection and transmission is observed at 556 cm^{-1} that is not attributed to the optical phonon modes. Numerical models predict a localized surface phonon polariton mode near this frequency, and we attribute the anomaly to coupling to this surface mode. The results of this work suggest that HfO_2 nanoparticles could enable engineered optical properties in new mid- and far-infrared materials and devices. *Published by AIP Publishing.* [http://dx.doi.org/10.1063/1.4991544]

Noble metal nanoparticles (NPs) have been the subject of intense research across myriad fields because of applications enabled in plasmonic sensing,[1] optical coatings,[2,3] circuits and optical metamaterials,[4–6] surface enhanced infrared absorption,[7] and surface enhanced Raman scattering.[8] These applications have enormous impacts on photonics and optics in the visible and near-infrared. Much of this progress is enabled by the tailored interaction of light with the NPs, which can be engineered by the controlling intrinsic and extrinsic properties of the NPs. A similar infrastructure for longer wavelengths could lead to new applications and improvements in sensing, imaging, and more. However, noble metal NPs are limited at longer wavelengths due to the large, negative permittivity, ϵ, of the metals.[9]

In the mid- and far-IR, away from interband transitions, coupling to collective oscillations of free-carriers, called plasmons, and vibrations of the crystal lattice in polar materials can significantly affect the permittivity of a material.[10,11] For commonly used noble metals, the large free-carrier density (5.9×10^{22} cm^{-3} for Au[12]) results in a plasma frequency in the visible or near-infrared and $\mathrm{Re}(\epsilon) \ll 0$ in the mid-IR.[9] One strategy to engineer $\mathrm{Re}(\epsilon)$ in the long-wavelength IR is to use doped semiconductors to control the free-carrier density and thus the permittivity.[13] While reducing the free-carrier density is a viable strategy for a portion of the mid-IR, vibrations of the crystal lattice (phonons) eventually dominate the optical characteristics of most polar crystals at longer wavelengths.[10,11] In the so-called *Reststrahlen* band, the spectral region between the longitudinal optical (LO) and transverse optical (TO) phonons, $\epsilon < 0$, and nanostructures and NPs made from these materials can support localized modes similar to localized surface plasmons in the field of plasmonics.[10,11,14,15]

Hafnium dioxide (HfO_2) is a polar crystal with a *Reststrahlen* band in the mid- and far-infrared. HfO_2 is already used in many photonic and electronic applications including optical coatings,[16,17] interference filters and dielectric mirrors,[18–20] thermal barrier coatings,[21,22] and field-effect transistors.[23,24] HfO_2 has many polymorphs (cubic, orthorhombic, and monoclinic) at atmospheric pressure; however, at temperatures below 2000 K, the most stable form is monoclinic HfO_2 (m-HfO_2).[25] m-HfO_2 exhibits optical phonon modes in the mid- and far-IR spectral regions (~130–800 cm^{-1}). The optical characterization of HfO_2 polymorphs has thus far been limited to thin films[16,17,19,21,23,26–29] where the optical spectra exhibit a few dominant phonon modes and are highly dependent on the crystallographic direction and the experimental setup.[30–32]

In this manuscript, we characterize m-HfO_2 NPs with nominal diameters of 9, 30, and 45 nm in the mid- to far-IR portion of the electromagnetic spectrum (250–1200 cm^{-1}). In the *Reststrahlen* band of m-HfO_2, we observe strong absorption from the IR-active optical phonon modes. The frequencies of these modes agree well with the phonon energies predicted in the literature. Additionally, we observe an anomaly in the reflection and transmission measurements, which is not explained by coupling to an optical phonon. We attribute this anomaly to coupling to a localized surface phonon polariton (LSPhP) in HfO_2 NPs and provide a simple model that supports this claim.

HfO_2 NPs with nominal diameters of 9, 30, and 45 nm are prepared by a sol-gel process.[33] Aqueous reaction solutions are prepared by adding 0.208 M hafnium chloride to 24 ml of 2.08 M citric acid and stirred overnight to ensure complete dissolution. Ethylene glycol (0.2 M) is added to the solution under continuous stirring for 3 h at 90 °C to boil off excess water. The resulting gel is calcined in a preheated furnace at 650 °C for 2 h, 950 °C for 2 h, or 950 °C for 8 h to pyrolize the remaining organics and crystallize HfO_2 NPs with nominal diameters of ~9, ~30, or ~45 nm, respectively. The resulting HfO_2 powders are ground using a mortar and pestle prior to further preparations and characterization. The crystallographic phase of the as-synthesized NPs is monoclinic as determined using powder X-ray diffraction,[33] and

a)Author to whom correspondence should be addressed: odomingu@nd.edu.

the measured Raman spectra agree well with the spectra predicted from density function perturbation theory (DFPT) for m-HfO_2.[30–32]

The morphology and size distribution of the synthesized HfO_2 NPs are characterized using transmission electron microscopy (TEM). Figure 1 shows the distribution of major and minor axes measured from approximately 100 NPs sampled for each nominal NP diameter reveals that as-prepared HfO_2 NPs were slightly ellipsoidal with mean (± standard deviation) major axis diameters of 9 (2), 31 (8), and 43 (17) nm.

Thin films containing HfO_2 NPs are prepared on gold and KBr substrates for optical characterization. To create the thin films, HfO_2 NPs are surface functionalized by adding 1.5–2 wt. % polyvinylpyrrolidone (PVP) to a suspension of 50 g/l of HfO_2 NPs in ethanol and dispersed by ultrasonication. For films on KBr substrates that are appropriate for transmission measurements, suspension drops are pipetted on a 13 mm diameter KBr window and spread using a wire-wound rod.[34] Samples for reflection measurements are prepared in a similar fashion on $2 \times 2\,cm^2$ gold mirrors. For both substrates, the NPs form films—as verified using scanning electron microscopy—with less than a monolayer of complete coverage.

Angle-, wavelength-, and polarization-dependent transmission and reflection measurements are conducted from 250 to 7000 cm^{-1} using a Bruker Vertex 80 vacuum Fourier transform infrared spectrometer (FTIR). The measurements are performed in the internal sample compartment under vacuum to minimize atmospheric absorption. A room-temperature DLaTGS detector and a globar are used for all of the measurements. KBr and Mylar beamsplitters are used for the mid- and far-infrared measurements, respectively, and a linear polarizer is used to select the transverse magnetic (TM) or transverse electric (TE) polarization of light. Spectra are collected using a resolution of 3 cm^{-1} and averaged over 200 scans. We estimate that we measure 500×10^9 and 2×10^9 NPs for reflection and transmission measurements, respectively (Fig. 1).

Figure 2(a) depicts the measured transmission of 30 nm HfO_2 NPs on a KBr window (red) with the calculated transmission of a 30 nm HfO_2 thin film, obtained using previously published data for the permittivity[29] and a transfer matrix method (blue). More absorption features are observed in the NP spectrum compared with the thin film due to the anisotropy of the HfO_2 permittivity and the distribution of NP crystal orientations with respect to the incident light.

Angle-dependent reflectance spectra for TM polarized light are depicted in Figs. 2(b)–2(d) for NPs with nominal diameters of 9, 30, and 45 nm. All of the spectra exhibit dips at frequencies below 850 cm^{-1} and a monotonic decrease in reflectance beyond 850 cm^{-1}. The absorption dips, at low frequencies, are primarily due to optical phonon modes in the NP, while at high frequencies, the transmission behavior is attributed to Rayleigh scattering effects. The decrease in transmission with increasing frequency does not follow the expected λ^{-4} dependence, but similar effects have been reported in the mid-infrared region with Si NPs of comparable size.[35] This deviation from the expected behavior is attributed to empty space between NPs and complex interactions between the NPs and the substrate.

The reflection and transmission spectra of m-HfO_2 NPs are understood by considering the IR-active optical phonons. Fifteen IR phonon modes are expected, and their resonance frequency, oscillator strength, and damping constant can be estimated using DFPT.[26] The lowest frequency mode[17] is not observed in our measurements due to spectral cutoff dictated by the KBr substrate, but all other modes are visible. Figure 3(a) shows the average and standard deviation of the measured transmission for normally incident light obtained by characterizing six samples comprising 30 nm NPs that were separately prepared and measured. Moreover, the 30 nm NPs were also sampled from two separate syntheses. The measured spectra for all six samples exhibit similar peaks and dips in transmission. There is some difference in the values of the extrema and the overall transmission due to differences in sample preparation, primarily NP density and film thickness.

In general, dips in the transmission correspond to absorption by a phonon mode, allowing the phonon energies

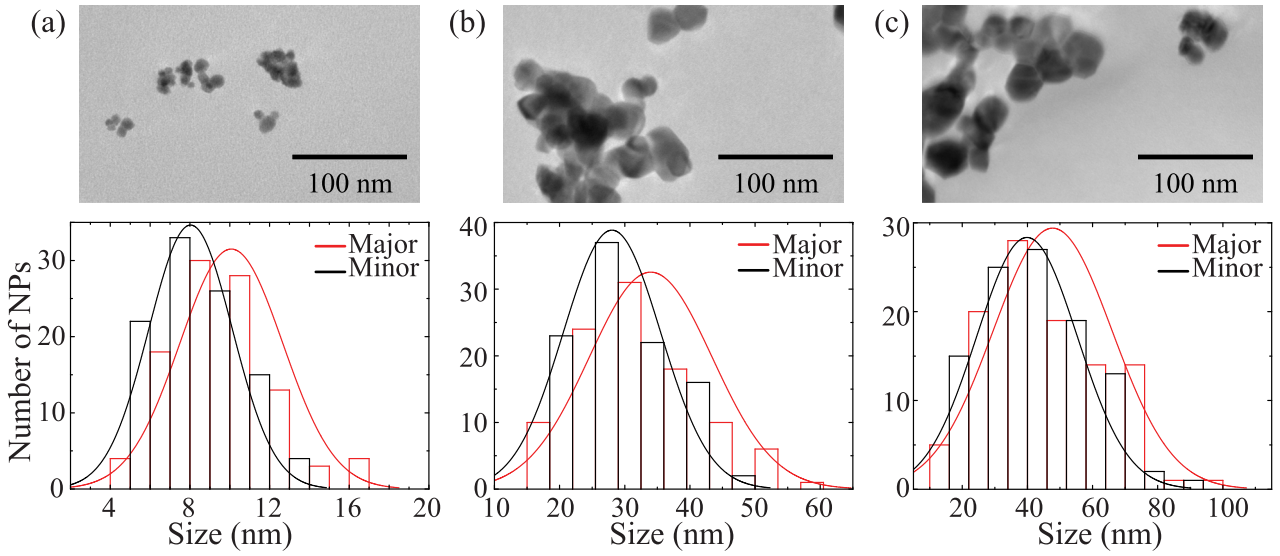

FIG. 1. Representative TEM micrographs and the measured distribution of major and minor axes of HfO_2 NPs exhibiting nominal diameters of (a) 9 nm, (b) 30 nm, and (c) 45 nm.

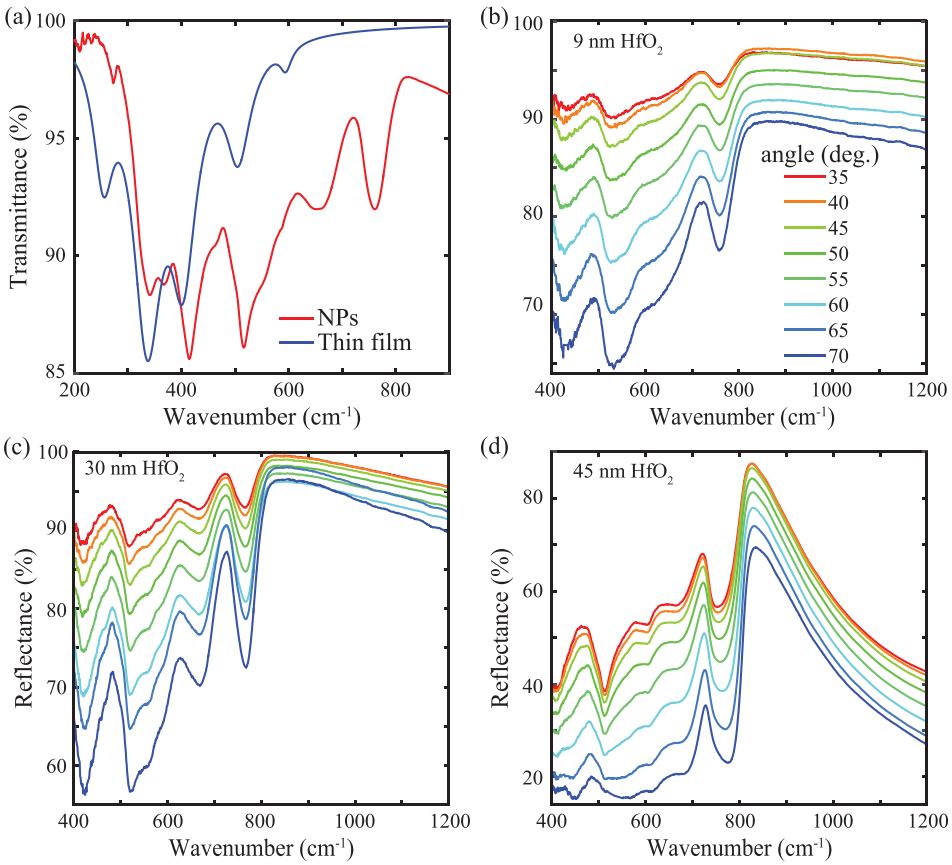

FIG. 2. (a) Transmission measurement (red) of 30 nm HfO_2 NPs on a KBr window and simulated transmission of a 30 nm thick HfO_2 film, calculated using the permittivity from Ref. 29. TM reflection measurements for samples comprising (a) 9 nm, (b) 30 nm, and (c) 45 nm HfO_2 NPs deposited on a gold mirror surface at various angles of incidence.

to be determined by fitting the spectral measurements. To identify various spectral features, we fit the measured transmission data with a simulated curve that is calculated using a transfer matrix code for a thin film with a multiple-oscillator model for the permittivity of the film.[36] We note that due to anisotropy that arises from the monoclinic crystal structure, the permittivity should be described using a tensor; however, because of the random orientation of the NPs in the thin films, anisotropy in the permittivity primarily broadens transmission dips. The permittivity in the mid- to far-IR is described using the following equation:

$$\varepsilon(\omega) = \varepsilon_\infty + \sum_j \frac{\omega_{pj}^2}{\omega_j^2 - \omega^2 - i\gamma_j\omega}, \tag{1}$$

where ε_∞ is the high frequency limit dielectric constant; the sum is over all IR-active optical phonon modes; ω_j, ω_{pj}, and γ_j are the resonance frequency, oscillator strength, and damping constant of the jth oscillator, respectively. We use ε_∞, ω_j, ω_{pj}, and γ_j as fitting parameters and limit the range of ω_j to $\pm 5\%$ of the predicted phonon energies in Ref. 26 in the fitting algorithm. We fit the measured data from 400 to 800 cm^{-1} for three different samples comprising 9, 30, or 45 nm NPs using a least squares method with the measured transmission and the simulated transmission calculated using a transfer matrix code. Table I summarizes the HfO_2 IR phonon modes from the literature,[30] and the mean and standard deviation of the recovered phonon resonance frequencies for the samples fit using this procedure. There is good agreement between the recovered phonon frequencies across the samples comprising 9, 30, and 45 NPs as evidenced by the small standard deviations and with the values reported in Ref. 26 and also between $\varepsilon_\infty = 3.74$ and the value reported in Ref. 29.

The measured transmission and the calculated fit from 400 to 800 cm^{-1} are shown in Fig. 3(b) for a sample comprising 30 nm NPs. The vertical dashed lines and shaded regions indicate the mean and standard deviation of the recovered phonon resonance frequencies from Table I, respectively. There is good agreement between the measurement and model over the majority of the spectral region; however, there is some deviation around 556 cm^{-1} where an anomalous dip in the transmission is observed in the measurement that is not predicted by the model. This anomalous dip in transmission is consistently observed in samples comprising 30 nm NPs (Fig. 3(a)). As shown in Table I, no optical phonons are predicted in this portion of the spectrum. Furthermore, the phonons that are energetically close to the anomalous region describe observed dips in the transmission. Therefore, attributing this anomaly to a phonon is not consistent with the already strong agreements between our measurements and previously published results—both the experiment and theory. Control measurements using PVP on a KBr window verify that the anomaly is not due to absorption by the PVP coating on the NPs. In addition to the anomaly at 556 cm^{-1}, there is also disagreement around 720 cm^{-1}. We believe that the disagreement is a result of increased Rayleigh scattering and the limitations of our simplified permittivity. However, we note that the measured phonon modes at 667 and 760 cm^{-1} do agree well with previous calculations and measurements.

We therefore attribute the dip in transmission around 556 cm^{-1} to coupling to localized surface phonon polaritons

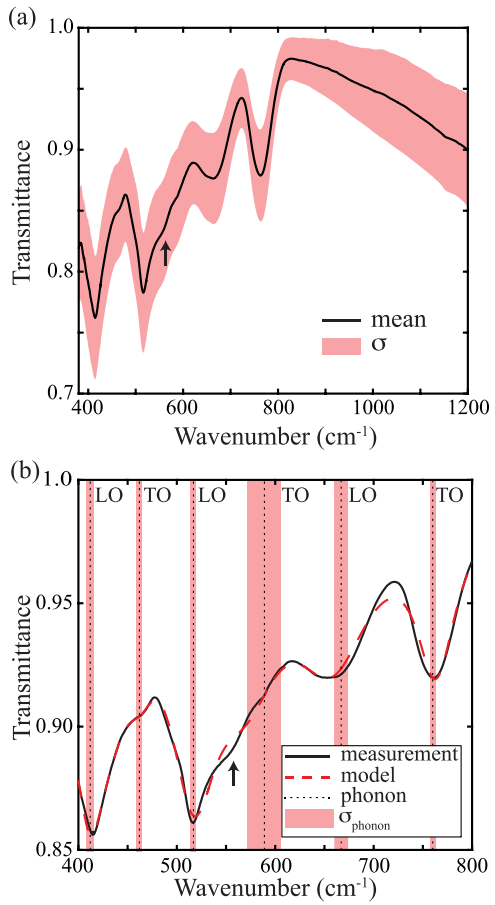

FIG. 3. (a) Mean (black line) and standard deviation (red shading), σ, of the measured transmittance for 6 samples comprising 30 nm HfO_2 NPs. The black arrow indicates the observed anomaly. (b) Measured transmission (black line) for 30 nm HfO_2 NPs with the calculated fit (dashed red line). The mean and standard deviation of the recovered phonon frequencies are indicated by vertical dotted lines and red shaded regions, respectively. The black arrow indicates the observed anomaly. The type of phonon is indicated with a label to the right of each dashed line using data from Ref. 31.

(LSPhP) on the NPs, which would not be predicted by our thin film model used to recover phonon energies. To support our claim, we calculate the expected frequency for the LSPhP using an electron-phonon microscopic model for polar optical phonons that describes localized modes in spherical particles using a lumped oscillator model for the permittivity.[29] The frequency of the LSPhP, ω_{LSPhP}, for spherical NPs within a surrounding medium, the so-called Frölich mode, is given as[37]

$$\omega_{\mathrm{LSPhP}} = \sqrt{\omega_{\mathrm{TO}}^2 \frac{\varepsilon_0 + 2\varepsilon_m}{\varepsilon_\infty + 2\varepsilon_{\mathrm{m}}}}, \tag{2}$$

TABLE I. Recovered parameters for the multiple-oscillator model of HfO_2.

Phonon frequency from Ref. 26 (cm^{-1})	Mean measured resonance frequency, ω_j (cm^{-1})	Standard deviation, σ_i (cm^{-1})
410	412	4
498	462	3
512	517	3
600	589	17
665	667	7
730	760	3

where $\varepsilon_\infty = 3.74$ and $\varepsilon_0 = 18$[38] are the high frequency limit dielectric constant and the static dielectric constant of HfO_2, respectively; $\varepsilon_m = 2.33$ is the dielectric constant of KBr;[36] and $\omega_{TO} = 336.5\,\mathrm{cm}^{-1}$ is the effective TO phonon mode in a lumped oscillator model. We obtain ω_{TO} by fitting the experimental reflection data with a single-oscillator, as in in Ref. 29. Using the values mentioned above, the calculated frequency of the LSPhP is $553\,\mathrm{cm}^{-1}$, which is close to the value of the anomaly observed on the 30 nm NPs.

The anomaly attributed to coupling to the LSPhP is consistently observed for the 30 nm NPs (Fig. 3(a)); however, for samples prepared using 9 and 45 nm NPs, the anomaly is only observed for some samples, and when it is observed, the dip is small compared to the 30 nm NP samples. We believe that this difference between samples is due to variability in the uniformity of deposited NP thin films as confirmed using scanning electron microscopy. To verify that better NP dispersion results in a strong dip in transmission, we prepare several samples of 45 nm NPs in a KBr matrix using a mortar and pestle to reduce NP agglomeration and measure the transmission through the sample, and for these samples, the anomaly at $556\,\mathrm{cm}^{-1}$ is visible as shown in Fig. 4. While NP size influences the frequency of the localized mode, the predicted shift in frequency for 30 and 45 nm diameter NPs is less than 0.01%. Additionally, a shift due to differences in the aspect ratio of the 30 and 45 nm NPs is also estimated using the Mie scattering theory to be small.[36]

In conclusion, monoclinic HfO_2 NPs with nominal diameters of 9, 30, and 45 nm are synthesized using a sol-gel method, and optical properties are characterized across the mid- and far-IR. Reflection and transmission measurements exhibit optical features that can be associated with coupling to optical phonon modes. The identified optical phonon modes are in good agreement with phonon modes predicted by DFPT. However, an anomaly in reflection and transmission is observed around $556\,\mathrm{cm}^{-1}$ that is not explained by coupling to an optical phonon. We present a simple model that predicts LSPhP modes around this frequency and argue that the anomaly is due to coupling to these modes. Further work is needed to improve the uniformity of deposited films in order to improve coupling to LSPhP modes on single NPs.

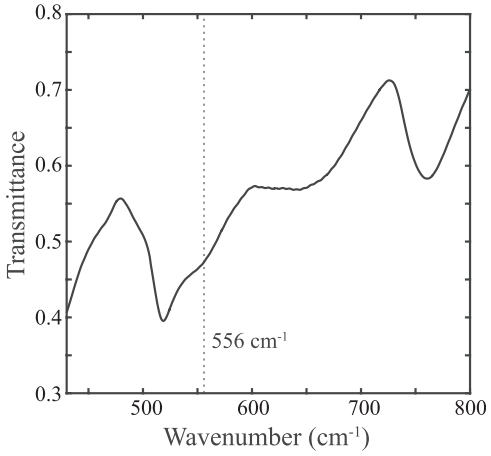

FIG. 4. Measured transmission for 45 nm HfO_2 NPs prepared in a KBr matrix.

Therefore, this work demonstrates the potential for using polar crystal NPs in the mid- and far-IR as an analog of noble metal NPs in the visible. These polar NPs could lead to improved sensing and materials for this important part of the spectrum.

This work was supported in part by funding from DARPA (FA8650-15-C-7546) and NSF (ECCS-1609362, DMR-1309587).

[1]P. Nyga, V. Drachev, M. Thoreson, and V. Shalaev, "Mid-IR plasmonics and photomodification with Ag films," Appl. Phys. B **93**, 59–68 (2008).
[2]T. Ning, Y. Zhou, H. Shen, H. Lu, Z. Sun, L. Cao, D. Guan, D. Zhang, and G. Yang, "Large third-order optical nonlinearity of periodic gold nanoparticle arrays coated with ZnO," J. Phys. D: Appl. Phys. **40**, 6705–6708 (2007).
[3]M. Mennig, K. Endres, M. Schmitt, and H. Schmidt, "Colored coatings on eye glass lenses by noble metal colloids," J. Non-Cryst. Solids **218**, 373–379 (1997).
[4]N. Engheta, "Circuits with light at nanoscales: Optical nanocircuits inspired by metamaterials," Science **317**, 1698–1702 (2007).
[5]Z. Li, S. Butun, and K. Aydin, "Touching gold nanoparticle chain based plasmonic antenna arrays and optical metamaterials," ACS Photonics **1**, 228–234 (2014).
[6]T. Sandu, D. Vrinceanu, and E. Gheorghiu, "Surface plasmon resonances of clustered nanoparticles," Plasmonics **6**, 407–412 (2011).
[7]F. Verger, T. Pain, V. Nazabal, C. Boussard Pledel, B. Bureau, C. Boussard Plédel, F. Colas, E. Rinnert, K. Boukerma, C. Compère, S. Ollivier, M. Guilloux Viry, S. Deputier, A. Perrin, and J. P. Guin, "Surface enhanced infrared absorption (SEIRA) spectroscopy using gold nanoparticles on As_2S_3 glass," Procedia Eng. **25**, 1645–1648 (2011).
[8]K. A. Willets and R. P. Van Duyne, "Localized surface plasmon resonance spectroscopy and sensing," Annu. Rev. Phys. Chem. **58**, 267 (2007).
[9]Y. Zhong, S. D. Malagari, T. Hamilton, and D. Wasserman, "Review of mid-infrared plasmonic materials," J. Nanophotonics **9**, 093791 (2015).
[10]K. Feng, W. Streyer, Y. Zhong, A. J. Hoffman, and D. Wasserman, "Photonic materials, structures and devices for Reststrahlen optics," Opt. Express **23**, A1418 (2015).
[11]J. D. Caldwell, L. Lindsay, V. Giannini, I. Vurgaftman, T. Reinecke, S. A. Maier, and O. Glembocki, "Low-loss, infrared and terahertz nanophotonics using surface phonon polaritons," Nanophotonics **4**, 44–68 (2015).
[12]N. W. Ashcroft, N. D. Mermin, and R. Smoluchowski, "Solid state physics," Phys. Today **30**(1), 61–65 (1977).
[13]T. Taliercio, V. N. Guilengui, L. Cerutti, J. B. Rodriguez, E. Tournie, V. Ntsame Guilengui, and E. Tournié, "All-semiconductor plasmonics for mid-IR applications," Proc. SPIE **8807**, 880702 (2013).
[14]M. Pelton, J. Aizpurua, and G. Bryant, "Metal-nanoparticle plasmonics," Laser Photonics Rev. **2**, 136–159 (2008).
[15]T. Low, A. Chaves, J. D. Caldwell, A. Kumar, N. X. Fang, P. Avouris, T. F. Heinz, F. Guinea, L. Martin-Moreno, and F. Koppens, "Polaritons in layered two-dimensional materials," Nat. Mater. **16**, 182–194 (2017).
[16]R. B. Tokas, S. Jena, S. Thakur, and N. K. Sahoo, "Effect of angle of deposition on micro-roughness parameters and optical properties of HfO_2 thin films deposited by reactive electron beam evaporation," Thin Solid Films **609**, 42–48 (2016).
[17]J. P. Lehan, Y. Mao, B. G. Bovard, and H. A. Macleod, "Optical and microstructural properties of hafnium dioxide thin films," Thin Solid Films **203**, 227–250 (1991).
[18]H. Jiao, X. Cheng, G. Bao, J. Han, J. Zhang, Z. Wang, M. Trubetskov, and A. V. Tikhonravov, "Study of HfO_2/SiO_2 dichroic laser mirrors with refractive index inhomogeneity," Appl. Opt. **53**, A56–A61 (2014).
[19]L. Smalakys, G. Bataviciute, E. Pupka, and A. Melninkaitis, "Comprehensive studies of IR to UV light intensification by nodular defects in HfO_2/SiO_2 multilayer mirrors," Proc. SPIE **9237**, 92371I (2014).
[20]J. Wang, S. Schroeder, M. Trost, M. Hauptvogel, and A. Duparre, "Angle resolved backscatter of HfO_2/SiO_2 multilayer mirror at 1064 nm," Proc. SPIE **9453**, 94530T (2015).
[21]K. Matsumoto, Y. Itoh, and T. Kameda, "EB-PVD process and thermal properties of hafnia-based thermal barrier coating," Sci. Technol. Adv. Mater. **4**, 153–158 (2003).
[22]J. Wang, H. Li, and R. Stevens, "Hafnia and hafnia-toughened ceramics," J. Mater. Sci. **27**, 5397–5430 (1992).
[23]V. Fiorentini and G. Gulleri, "Theoretical evaluation of zirconia and hafnia as gate oxides for Si microelectronics," Phys. Rev. Lett. **89**, 266101 (2002).
[24]C. Moldovan, R. Iosub, M. Modreanu, D. Ulieru, B. Firtat, and M. Ion, "ISFET microsensors HfO_2 based for biomedical applications," in International Semiconductor Conference (2006), Vol. 1, pp. 185–188.
[25]R. Terki, G. Bertrand, H. Aourag, and C. Coddet, "Cubic-to-tetragonal phase transition of HfO_2 from computational study," Mater. Lett. **62**, 1484–1486 (2008).
[26]D. Franta, I. Ohlídal, D. Nečas, F. Vižd'a, O. Caha, M. Hasoň, and P. Pokorný, "Optical characterization of HfO_2 thin films," Thin Solid Films **519**, 6085–6091 (2011).
[27]F. L. Martínez, M. Toledano-Luque, J. J. Gandía, J. Cárabe, W. Bohne, J. Röhrich, E. Strub, and I. Mártil, "Optical properties and structure of HfO_2 thin films grown by high pressure reactive sputtering," J. Phys. D: Appl. Phys. **40**, 5256–5265 (2007).
[28]M. Al-Kuhaili, "Optical properties of hafnium oxide thin films and their application in energy-efficient windows," Opt. Mater. **27**, 383–387 (2004).
[29]T. J. Bright, J. I. Watjen, Z. M. Zhang, C. Muratore, and A. A. Voevodin, "Optical properties of HfO_2 thin films deposited by magnetron sputtering: From the visible to the far-infrared," Thin Solid Films **520**, 6793–6802 (2012).
[30]R. Wu, B. Zhou, Q. Li, Z. Jiang, W. Wang, W. Ma, and X. Zhang, "Elastic and vibrational properties of monoclinic HfO_2 from first-principles study," J. Phys. D: Appl. Phys. **45**, 125304 (2012).
[31]B. Zhou, H. Shi, X. D. Zhang, Q. Su, and Z. Y. Jiang, "The simulated vibrational spectra of HfO_2 polymorphs," J. Phys. D: Appl. Phys. **47**, 115502 (2014).
[32]X. Zhao and D. Vanderbilt, "First-principles study of structural, vibrational, and lattice dielectric properties of hafnium oxide," Phys. Rev. B **65**, 233106 (2002).
[33]T. L. McGinnity, O. Dominguez, T. E. Curtis, P. D. Nallathamby, A. J. Hoffman, and R. K. Roeder, "Hafnia (HfO_2) NPs as an X-ray contrast agent and mid-infrared biosensor," Nanoscale **8**, 13627–13637 (2016).
[34]S. Jeong, L. Hu, H. R. Lee, E. Garnett, J. W. Choi, and Y. Cui, "Fast and scalable printing of large area monolayer NPs for nanotexturing applications," Nano Lett. **10**, 2989 (2010).
[35]V. G. Kravets, C. Meier, D. Konjhodzic, A. Lorke, and H. Wiggers, "Infrared properties of silicon nanoparticles," J. Appl. Phys. **97**, 084306 (2005).
[36]C. F. Bohren and D. R. Huffman, *Absorption and Scattering of Light by Small Particles* (Wiley, 1983).
[37]E. Roca, C. Trallerogine, and M. Cardona, "Polar optical vibrational-modes in quantum dots," Phys. Rev. B **49**, 13704–13711 (1994).
[38]S. Kar, *High Permittivity Gate Dielectric Materials* (Springer, Heidelberg, 2013), p. 163.